Disk-crossing Orbits

C. Hunter

Department of Mathematics, Florida State University,
Tallahassee FL 32306-4510, USA

Abstract. We study orbits in simplified models of galaxies which consist of two components, a disk and a halo. The disk is idealized as razor-thin, though we present evidence that this simplifying assumption is not critical. We find that the presence of the disk causes many more resonances than have been found in similar smooth potentials. Those resonances grow at relatively modest values of energy, overlap, and give rise to many stochastic orbits. A significant range of regular orbits remain and show smooth KAM curves, even though the discontinuous potential due to the razor-thin disk means that current versions of the KAM theorem do not apply.

1 Introduction

Many galaxies have a disk component and one or more other components which are much less flattened. Normal spirals and S0s are examples. Bender et al [1] have found that many ellipticals can be classified as disky, and that their diskiness is consistent with a disk plus bulge model [2]. For simplicity, we use halo as an all-embracing term to describe the whole non-disk component. Orbits of halo stars in such galaxies will necessarily cross back and forth through the disk. As they do, they will experience a fairly abrupt change in the gravitational force field. This paper examines how these changes in the force field affect the dynamics of the orbit. It is a topic which seems to have attracted very little attention so far, with two notable exceptions. Ostriker, Spitzer, and Chevalier [3] have discussed the effect that the compressive gravitational shocks, caused by passage through the disk, have on the internal structure of globular clusters. Our interest is on how that passage affects the orbits of individual stars of the halo population, on the resonances which they can cause, and on the extent to which they can induce chaos. This issue was also studied in the 1970s by L. Martinet and co-authors [4]–[7] who integrated orbits in Schmidt's [8], [9] two models of the Galaxy. These models have highly flattened disk components.

We shall use simple models which have both disk and halo components. These are the Kuzmin-like potentials which were introduced recently by Tohline and Voyages [10]. Their disk components are razor-thin. We describe their potentials and densities in Sect. 2, and their dynamics in Sect. 3. Numerical integrations are needed to study the detailed properties of orbits. We describe the results of those integrations in Sect. 4. In Sect. 5 we show, again by means of orbit integrations, that our findings do not depend critically on the simplifying approximation that the disk component is razor-thin. Sect. 6 sums up, and relates our findings to other work.

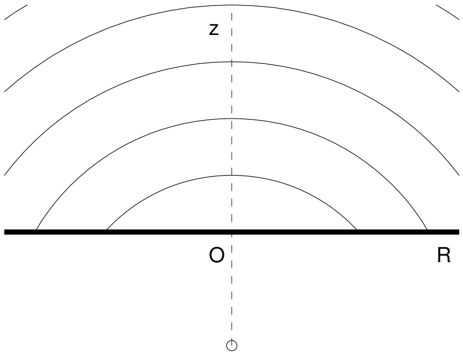

Fig. 1. The thin solid lines in $z > 0$ are equipotential surfaces above Kuzmin's disk. They are circles in (R, z)-space centered on an image mass at $z = -a$, which is shown as a small open circle. The equipotentials in $z < 0$ are their reflections in the disk $z = 0$

2 Models

2.1 Kuzmin's Disk

Kuzmin's disk [11] [12] is a flat density distribution with the remarkable property that the gravitational potential above it is that due to a point mass at a distance a below it, while the potential below it is that due to a point mass at a distance a above it. Its gravitational potential is

$$\Phi = \frac{-GM}{\sqrt{R^2 + (a + |z|)^2}}, \tag{1}$$

when $z = 0$ is the plane of the disk, and R measures radial distance from the z-axis of symmetry. Its equipotential surfaces are spherical, those in $z > 0$ centered on the point mass below the disk, and those in $z < 0$ on the point mass above the disk.

2.2 Kuzmin-like Potentials

Kuzmin's disk is a particular case of the more general Kuzmin-like potentials of Tohline and Voyages [10], for which

$$\Phi = \Phi(\xi), \qquad \xi = \sqrt{R^2 + (a + |z|)^2}. \tag{2}$$

They have the same spherical equipotential surfaces as Kuzmin's disk, with centers of force on the opposite side of the $z = 0$ plane, but a force law which is more general than the inverse-square of Kuzmin's disk. The variable ξ measures distance from the centers of force. Poisson's equation shows that the potential (2) is generated by a density

$$\varrho = \frac{1}{4\pi G}\Delta\Phi = \frac{1}{4\pi G}\left[\Phi''(\xi) + \frac{2[1 + a\delta(z)]}{\xi}\Phi'(\xi)\right]. \tag{3}$$

The Dirac delta function $\delta(z)$ arises from derivatives of $|z|$ because $\partial|z|/\partial z = \mathrm{sgn}(z)$, and $\partial\,\mathrm{sgn}(z)/\partial z = 2\delta(z)$. Kuzmin-like potentials therefore arise from a volume density which is stratified on the equipotentials, together with a surface density $\sigma = a\Phi'(\xi)/2\pi G\xi$ on the plane $z = 0$. It is this surface density which causes the z-component of force to be discontinuous. The volume density vanishes for the special case of Kuzmin's disk, and there is then only a surface density $\varrho = aM\delta(z)/2\pi(a^2 + R^2)^{3/2}$.

The choice of a specific spherical potential $\Phi(\xi)$ fixes both the volume and the surface densities. One way of judging their relative significance is to compute the mass of each component interior to some equipotential $\xi = \xi_0$. Using the geometric formula of $4\pi\xi(\xi - a)$ for the surface area of the two part-spheres which form the equipotential of constant ξ, we obtain

$$M_{\mathrm{disk}}(\xi_0) = \frac{a}{G}\left[\Phi(\xi_0) - \Phi(a)\right], \qquad M_{\mathrm{total}}(\xi_0) = \frac{\xi_0}{G}(\xi_0 - a)\Phi'(\xi_0), \tag{4}$$

for the disk and total mass interior to the equipotential $\xi = \xi_0$.

2.3 The Logarithmic Kuzmin-like Potentials

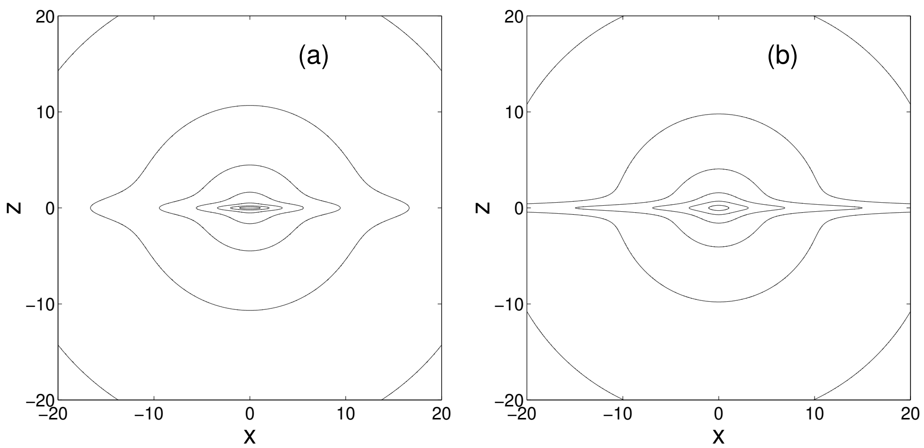

Fig. 2. (a) Projected density of a logarithmic Kuzmin-like model (5), assuming the same mass-to-light ratio for all mass, when viewed at 5° from edge-on (left). Contour levels decrease by factors of $10^{-1/3}$. The projected disk density is infinite when viewed edge-on, and the isophotes become increasingly less pointy as the viewing angle increases. (b) Projected density of the same model after thickening with $b = 0.5$ as described by (12) in Sect. 5 when viewed edge-on. The centermost contours and successive outer ones represent the same levels as in (a). Thickening spreads density out from the disk, giving higher volume densities; the level of the outermost contour of (b) matches the next to outermost of (a)

As an example, we shall investigate the logarithmic potential which is widely used as a model in galactic dynamics [12]. It gives a Kuzmin-like model with potential and density

$$\Phi(\xi) = V_0^2 \ln \xi, \quad \varrho = \frac{V_0^2}{4\pi G \xi^2} + \frac{a V_0^2 \delta(z)}{2\pi G (R^2 + a^2)}. \tag{5}$$

As (4) shows, the mass in the disk grows logarithmically with increasing distance whereas the total mass grows linearly. The ratio of these masses is

$$\frac{M_{\rm disk}(\xi_0)}{M_{\rm total}(\xi_0)} = \frac{a}{(\xi_0 - a)} \ln \left(\frac{\xi_0}{a} \right), \tag{6}$$

and the relative significance of the disk diminishes with increasing ξ_0. Orbits at higher energies and greater distances experience forces for which the halo is increasingly dominant. Figure 2-a shows how isophotes would appear when viewed at a small angle from edge-on, assuming the same mass-to-light ratio for all mass.

3 Dynamics

Motion in a spherical potential conserves the energy E and the angular momentum vector about the center. The motion is integrable and is confined to the plane through the center of force that is perpendicular to the angular momentum vector. Unless confined always to the plane $z = 0$, an orbit in a Kuzmin-like potential passes continually back and forth between the regions $z > 0$ and $z < 0$, and hence from one spherical potential field to the other. Different angular momenta are conserved in the two regions. Both are described by the vector

$$\mathbf{J} = [\mathbf{r} + a\,\mathrm{sgn}(z)\mathbf{k}] \times \mathbf{v}, \tag{7}$$

where $\mathbf{r}$ is the position relative to the origin, $\mathbf{v}$ is velocity, and $\mathbf{k}$ is the unit vector in the z-direction. An equation of motion for $\mathbf{J}$ can be derived from the equations of motion in the Kuzmin-like potential. They are

$$\frac{\mathrm{d}\mathbf{r}}{\mathrm{d}t} = \mathbf{v}, \qquad \frac{\mathrm{d}\mathbf{v}}{\mathrm{d}t} = -\nabla\Phi = -\frac{[\mathbf{r} + a\,\mathrm{sgn}(z)\mathbf{k}]}{\xi}\Phi'(\xi). \tag{8}$$

It follows that

$$\frac{\mathrm{d}\mathbf{J}}{\mathrm{d}t} = [\mathbf{r} + a\,\mathrm{sgn}(z)\mathbf{k}] \times \frac{\mathrm{d}\mathbf{v}}{\mathrm{d}t} + \mathbf{v} \times \mathbf{v} + 2a\delta(z)(\mathbf{k} \times \mathbf{v})\frac{\mathrm{d}z}{\mathrm{d}t} = 2a\delta(z)(\mathbf{k} \times \mathbf{v})\frac{\mathrm{d}z}{\mathrm{d}t}. \tag{9}$$

This equation confirms the constancy of the vector $\mathbf{J}$ except when the orbit crosses the disk. Then $\mathbf{J}$ changes discontinuously by an amount $\pm 2a(\mathbf{k} \times \mathbf{v})$ unless $\mathbf{k} \times \mathbf{v} = 0$, that is unless the orbit is then travelling perpendicularly to the disk. The change in $\mathbf{J}$ is always perpendicular to the z-direction because the z-component J_z of $\mathbf{J}$ is conserved; J_z is the angular momentum about the axis of symmetry, and is a constant of the motion, as in any axisymmetric potential. Since it is known that energy and angular momenta are the only constants of motion in general spherical potentials and, as we have seen, neither J_x nor J_y are conserved for general Kuzmin-like potentials, it follows that, contrary to what is stated in [10], Kuzmin-like potentials are not generally integrable. Kuzmin's disk is exceptional, its potential is Stäckel, and so all orbits in it are integrable. Their integrability relies on the Keplerian nature of its spherical potentials; motions then have an extra integral of motion, the Laplace-Runge-Lenz vector [13], in addition to energy and angular momentum. The Laplace-Runge-Lenz vector changes discontinuously across the disk too. However, there is a linear combination of its z-component and $\mathbf{J}^2$ for which the two discontinuities cancel [14], and this combination provides Kuzmin's third integral [11]. (Another exceptional case is that of a harmonic potential $\Phi \propto \xi^2$. It is not generally relevant for galaxies, except as an approximation for orbits which remain close to the center of the disk.)

Because position and velocity of an orbit are continuous as the disk is crossed, the tangent to an orbit changes smoothly. The hallmark of the discontinuity in the gravitational force is a discontinuity in the curvature of an orbit. Fig. 3-a gives the clearest example of this feature. It shows a particular $J_z = 0$ periodic polar orbit in the potential due to Kuzmin's disk. The orbit in $z < 0$ is part of an ellipse with focus at the center of force in $z > 0$. This ellipse is oriented such that the orbit is travelling directly away from the center of force in $z < 0$ as it crosses to $z > 0$. Hence its trajectory in $z > 0$ remains a straight line away from the lower center of force. The orbit travels along that line until it reaches the maximum extent which its energy allows, after which it returns and retraces its path.

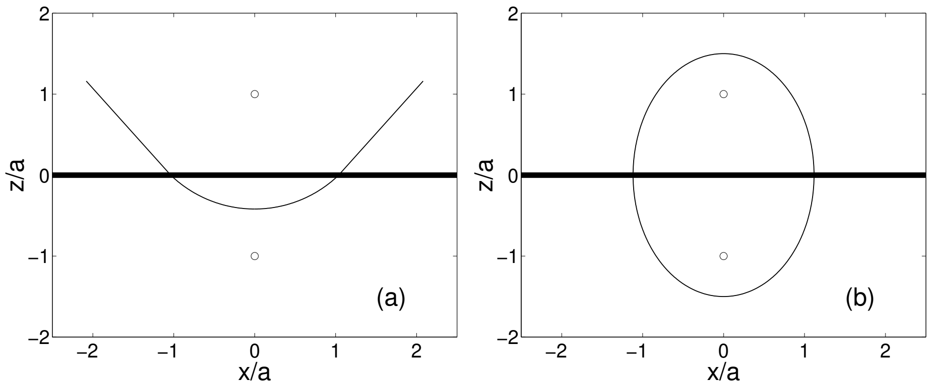

Fig. 3. The simplest periodic disk-crossing polar orbits for Kuzmin's disk: (a) a box orbit, which is a banana in the terminology of Binney [15] and a boxlet in the terminology of Miralda-Escudé and Schwarzschild [16], and (b) an ellipse, for energy $E = -GM/3a$. The open circles again denote the image masses as in Fig. 1. Similarly shaped periodic orbits occur for other Kuzmin-like potentials. The banana boxlet has a twin, which is its mirror image in $z = 0$.

4 Orbits

4.1 Orbits in Kuzmin's Disk

Orbits with $J_z \neq 0$ are short-axis tubes. Polar orbits with $J_z = 0$, which lie in planes through the axis of symmetry, may be either boxes or loops. At low energies $-1 < E < -GM/2a$ for which the orbit along the z-axis is stable, only box orbits occur. Loop orbits become possible at higher energies in the range $-GM/2a < E < 0$ for which the z-axis orbit has become unstable [14] The parent of the loop orbit family is a closed ellipse, as shown in Fig. 3-b. It is not quite a Keplerian ellipse because the orbit is always under the influence of a point mass at the more distant focus. Rather it is the union of two slower halves of a Keplerian ellipse. Although there are box orbits for all energies, the type of banana boxlet shown in Fig. 3-a occurs only for the energy range $-GM/2\sqrt{2}a \leq E < 0$. The curved part of the orbit is a quarter circle for the lower limit of energy, and so is nearly circular for the case illustrated. Its eccentricity increases as E increases, and the linear parts, which extend to a distance $-GM/E$ from the lower center of force, lengthen.

4.2 Orbits in Kuzmin-like Potentials

In the following subsections, we present numerical results for the logarithmic potential (5) using $z = 0$ surfaces of section. Surfaces of section for Kuzmin's disk can be found analytically as contours on which the third integral is constant, but numerical integration is needed for Kuzmin-like potentials. We computed orbits by a variant of the method described in Appendix A.1 of Hunter et al [17] which integrates accurately from one crossing of $z = 0$ to the next using polar coordinates in (z, v_z)-space. No interpolation is used to find when crossings occur, and there is no uncertainty as to which force formula to use. The surfaces of section for the logarithmic potential (5) contain resonant island chains and stochastic as well as regular regions. They stand in marked contrast to the regular surfaces of section for for Kuzmin's disk, for which the only significant feature is the bifurcation when loops first appear with polar orbits. Surfaces of section are plotted for specific values of energy and angular momentum J_z about the axis of symmetry. We express J_z as a fraction k of the angular momentum of the circular orbit in the z-plane., i.e. the maximum possible J_z for the given energy. We use a as unit of length, and for ease of understanding, identify energies by R_c, the radius of a circular orbit at that energy. In terms of R_c, the energy is

$$E = \frac{1}{2}\left[\ln(R_c^2 + 1) + \frac{R_c^2}{R_c^2 + 1}\right]. \tag{10}$$

For the unbounded potential (5), $E \geq 0$, and R_c increases monotonically with the energy, first as $R_c \approx \sqrt{E}$ for small E, but later as $R_c \approx e^E$ for large E. We label periodic orbits by the ratio $m : n$ where m and n are the numbers of the full cycles in z and R (or x in the case of polar orbits) respectively, in a complete cycle.

Polar Orbits

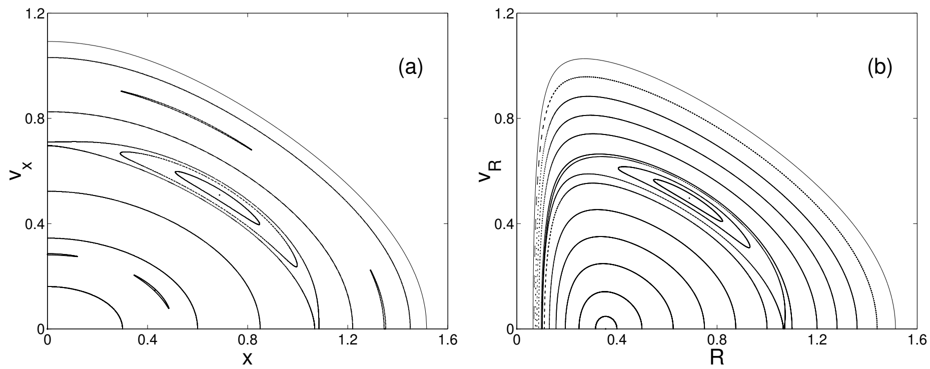

Fig. 4. (a) Surface of section for polar orbits in the logarithmic potential (5) for $R_c = 1$, (b) Surface of section for axisymmetric orbits in the same potential and at the same energy, and with $k = 0.1$, i.e. angular momentum 0.1 of that for a circular orbit at this energy

Only box orbits occur at low energies, and (x, v_x) surfaces of section mostly show smooth rings centered on the z-axis orbit at $(0, 0)$. However bifurcations do occur before the z-axis orbit becomes unstable at $R_c = 1.37$. Figure 4-a for $R_c = 1$ shows three rings of island chains. The prominent middle ring is due to the $2:1$ banana boxlets, and their unstable figure-of-eight companion. These orbits bifurcate from the z-axis orbit when $R_c = 0.62$. Initially their paths lie close to the z-axis, but their initial island chain cuts the z-axis at $z = 0.35$, and is clearly removed from $(0, 0)$. The smooth curves surrounding $(0, 0)$ remain, indicating that the stability of the z-axis orbit is unaffected by this bifurcation. The outer narrow ring corresponds to $3:1$ orbits. They bifurcate from the z-axis orbit at a lower energy when $R_c < 0.45$. The inner narrow ring corresponds to $3:2$ orbits of a well-known type; an unstable fish and a stable antifish [16]. A separatrix between box and loop orbits is formed once the z-axis orbit becomes unstable at $R_c = 1.37$, and a visible stochastic region develops around the separatrix [18]. Figure 5 shows that resonant islands take up a significant part of the box orbit region at $R_c = 3$. The $2:1$ banana boxlet at $x = 1.84$, $v_x = 1.15$ is still prominent, while the $3:2$ family with periodic points at $x = 2.54$, $v_x = 0.79$ and $x = 0$, $v_x = 1.14$ has grown in significance. Figure 6 shows that most of the box orbit region has become stochastic when energy has increased to $R_c = 10$, as a result of substantial overlapping of the resonant regions which are so prominent in Fig. 5. There are many resonant islands in Fig. 6, and even islands within islands, but the stochastic sea dominates the outer part of the surface of section. The island for the banana boxlets, which is here centered on $x = 3.2$, $v_x = 1.7$, has moved further outwards and become thinner. The outward migration is due to the fact that these orbits become flatter with increasing energy; the outer boundary of the surfaces of section is the orbit which is always in the plane $z = 0$. A few box orbits remain in the outer parts of the surface of section. They too are flat and never depart far from the $z = 0$ plane.

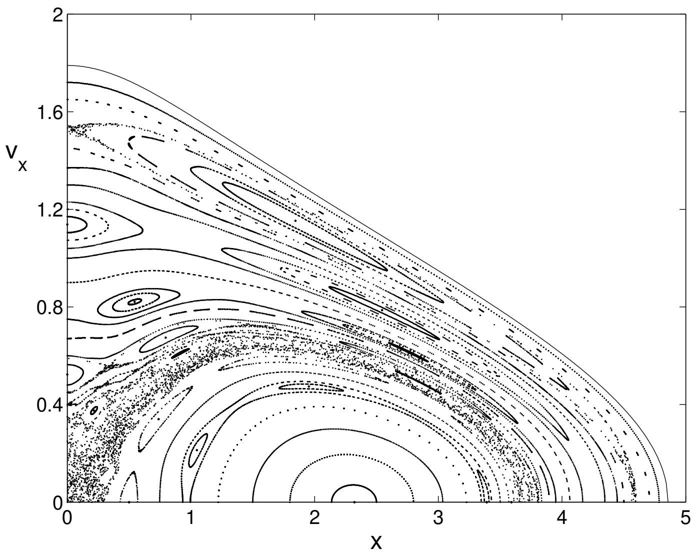

Fig. 5. Surface of section for polar orbits in the logarithmic potential (5) for $R_c = 3$

While the box orbit region is becoming stochastic, the loop orbit region, centered around the 1 : 1 periodic closed loop, remains largely regular, though with some resonant islands. The first out from the center and most prominent in Fig. 6 are due to the 2 : 2 periodic orbits whose three-petalled rosette form is shown in Fig. 7-a.

Delay Plots of Angular Momentum provide a third way of analyzing orbits in Kuzmin-like potentials, which supplement plots in position space and surfaces of section. While the orbit is above the disk, J_y is its angular momentum about the lower center of force, and remains constant. The next time the orbit returns to $z > 0$, it has a new value of J_y, except for exceptional cases such as the elliptical orbit of Fig. 3-b. The sequence of successive values of J_y characterizes an orbit, and generates a delay plot, similar to those used for analyzing time series generated by other dynamical systems [19] [20], in which two successive values are plotted as a point, the earlier value giving the abscissa and its successor the ordinate. Figure 8 displays J_y delay plots for four orbits which are included in the surface of section of Fig. 6. The physical forms of the first three are shown in Fig. 9. The orbits are arranged by decreasing stochasticity and increasing regularity. Orbit (a) inhabits the stochastic region just outside the regular central

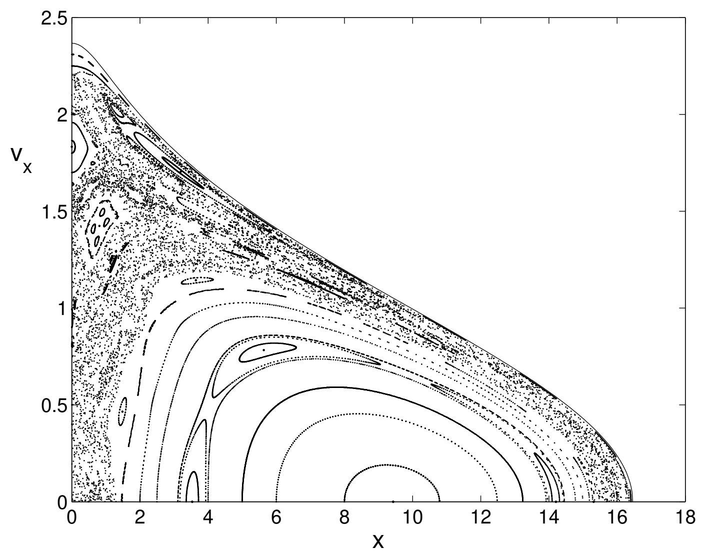

Fig. 6. Surface of section for polar orbits in the logarithmic potential (5) for $R_c = 10$

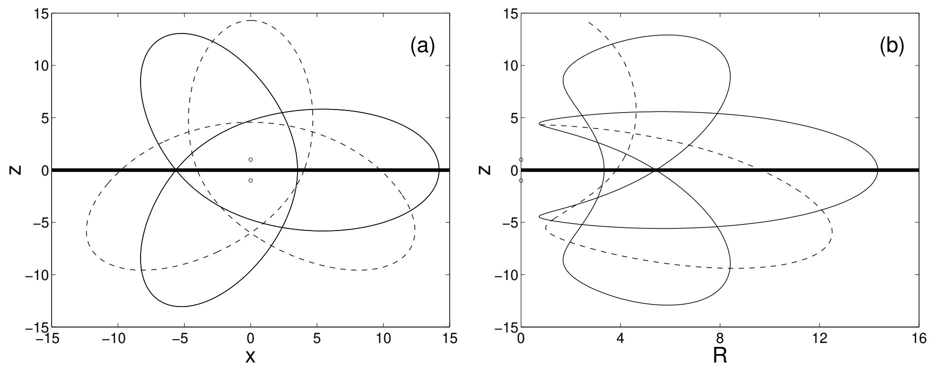

Fig. 7. (a) Stable and unstable 2 : 2 orbits, full and broken lines respectively, which occupy the centermost chain of islands in Fig. 6. The reflection of the unstable orbit in $z = 0$ gives another unstable 2 : 2 orbit. (b) The stable and unstable 2 : 4 orbits, full and broken lines respectively, which occupy the centermost chain of islands in Fig. 11

core of loop orbits. The points in its delay plot are scattered fairly uniformly. Figure 9-a shows that it almost fills the area within the zero-velocity curve, apart from narrow slivers near the left and right edges. Orbit (b) from well inside the stochastic region fills less than half the region within the zero-velocity curve. Its delay plot shows much randomness, but also a double ring structure. Orbit (c) is something of a surprise because it seems to start in a stochastic region, yet its delay plot is highly ordered. Its pretzel shape as seen in Fig. 9-c shows it to belong to the family of 4 : 3 periodic orbits parented by the periodic orbit which

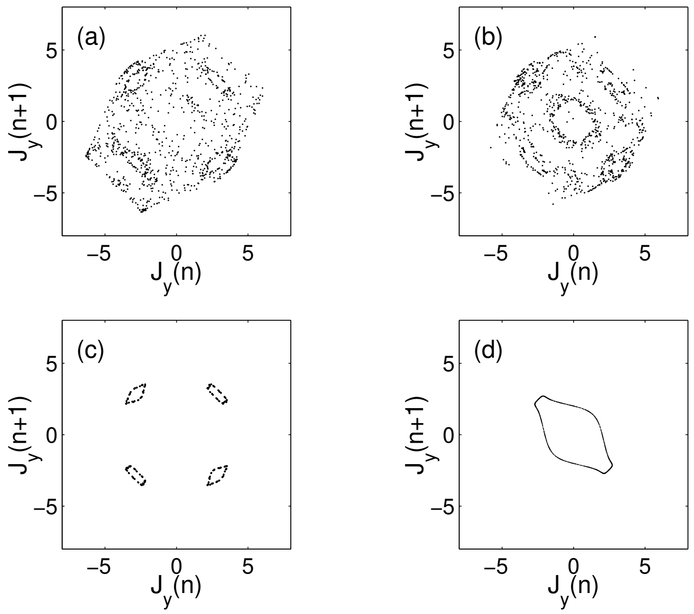

Fig. 8. J_y delay plots for four $R_c = 10$ polar orbits. $J_y(n)$ is the value of J_y during the n-th passage through $z > 0$. The orbits start in $z = 0$ from (a) $x = 2$, $v_x = 1$, (b) $x = 1$, $v_x = 1.7$, (c) $x = 4$, $v_x = 1.4$, (d) $x = 0$, $v_x = 2.25$

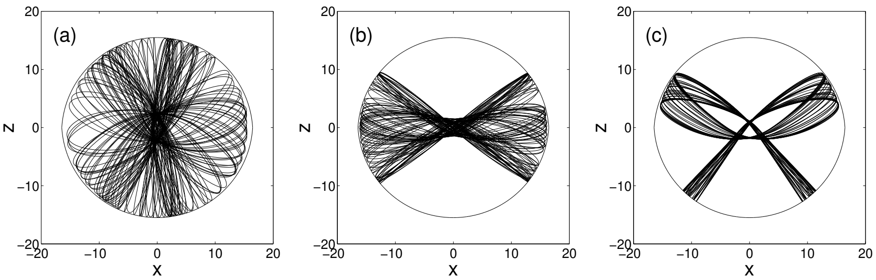

Fig. 9. Orbits for first three delay plots of Fig. 8, after 200 crossings of $z = 0$. The outer boundary is the zero-velocity curve

crosses the surface of section of Fig. 6 at $(0.81, 1.42)$ and $(6.38, 1.21)$. Orbit (c) generates the set of broken lines which surrounds the four island chain around $(0.81, 1.42)$, and broken lines appear in its delay plot too. The starting point of this orbit at $(4, 1.4)$ lies at the left end of a long and narrow island surrounding the other periodic point at $(6.38, 1.21)$. That island is lost in the complexity of Fig. 6. Finally, orbit (d) is a regular box orbit which gives a smooth curve around the outer part of the surface of section. Its delay plot is also smooth and regular. Being close to the outer boundary, this orbit is a flat box which stays close to the disk at all times.

Axisymmetric Orbits

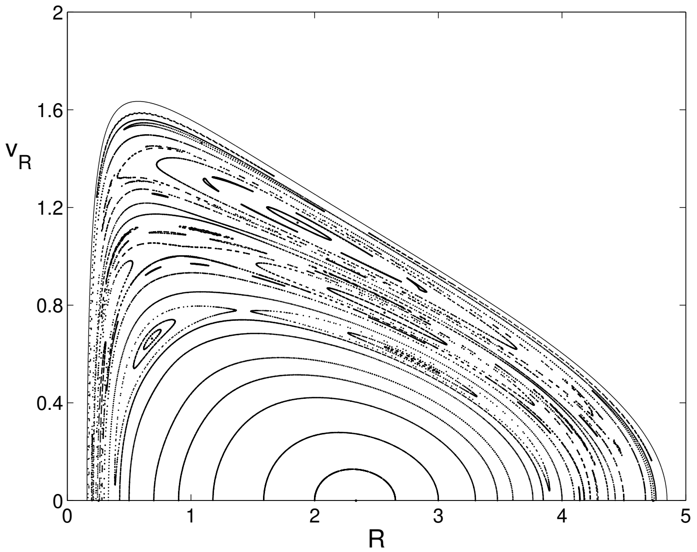

Fig. 10. Surface of section for axisymmetric orbits in the logarithmic potential (5) for $R_c = 3$ and $k = 0.1$

The surfaces of section Fig. 4-b, Fig. 10, and Fig. 11 for the same three energies of $R_c = 1, 3$, and 10, respectively, and for J_z angular momenta which are one-tenth of the maximum possible ($k = 0.1$) show similar trends with increasing energy to the corresponding figures for polar orbits. The predominant class of regular orbits are short axis tubes [14]. They give the smooth rings surrounding the center which represents a thin tube or shell. Figure 4-b shows a prominent island at the lowest energy. This is due to the $1:1$ saucer orbit [21] which is obtained when the angular momentum barrier stops a banana orbit before it gets to the z-axis and reflects it back along its path after its first crossing of the disk. The $R_c = 3$ surface of section in Fig. 10 shows its outer part to be occupied by resonant island chains. Those resonances have overlapped when the energy has increased to $R_c = 10$, and most of the outer part is stochastic. However there is a large regular core with a prominent island chain. That chain corresponds to the axisymmetric counterparts of the $2:2$ rosettes of the polar case. The angular momentum barrier truncates and reflects these orbits to give the $2:4$ orbits shown in Fig. 7-b, a stable spaceship and an unstable pair of twisted fish. Note that this island chain is present already as the innermost island chain in Fig. 10 for the lower energy of $R_c = 3$. There is a difference in that there the unsymmetric twisted fish are stable, and the spaceship is unstable.

Delay plots can be constructed for this case too, using the quantity $J_x^2 + J_y^2$ which is now constant during each passage through $z > 0$. Figure 12 shows delay

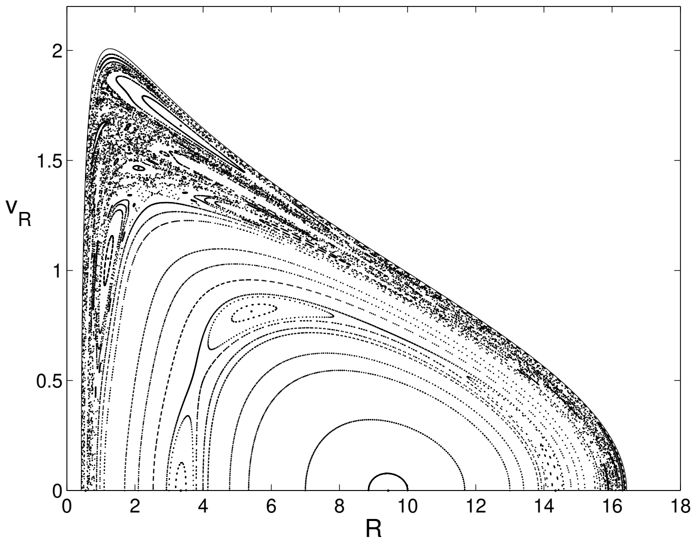

Fig. 11. Surface of section for axisymmetric orbits in the logarithmic potential (5) for $R_c = 10$ and $k = 0.1$

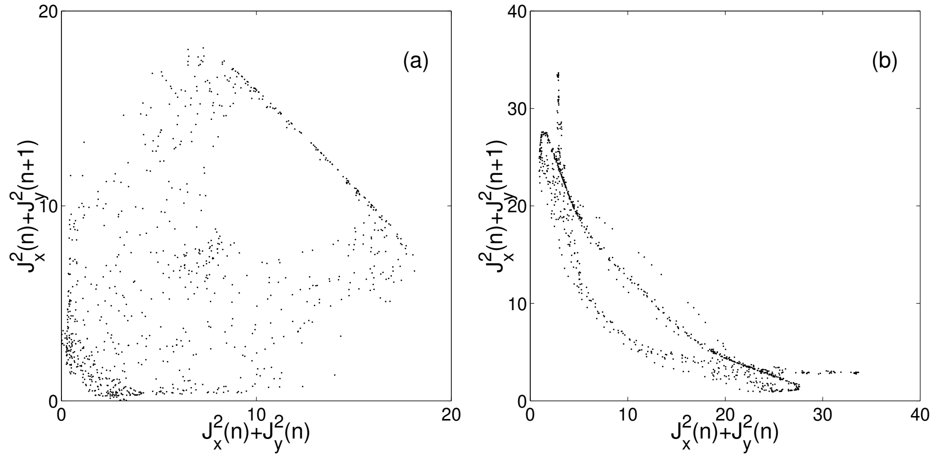

Fig. 12. $J_x^2 + J_y^2$ delay plots for two $R_c = 10$, $k = 0.1$ axisymmetric orbits. The orbits start in $z = 0$ from (a) $R = 1$, $v_R = 1.7$, (b) $R = 1.6$, $v_R = 1$

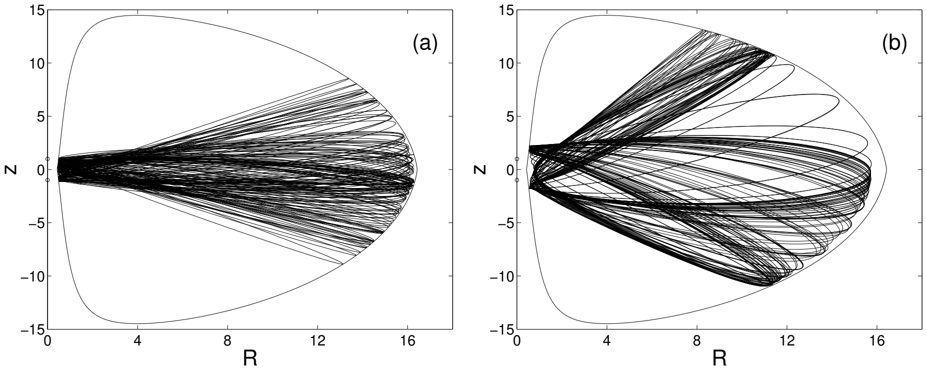

Fig. 13. Orbits for the two delay plots of Fig. 12 after 200 crossings of $z = 0$. The outer boundary is the zero-velocity curve

plots for two orbits from the outer stochastic part of Fig. 11. The left delay plot shows wide scattering, with some concentration at the boundaries, and an empty hole at the top right, while the right plot shows far less scattering. Figure 13 shows that neither orbit comes close to filling the region within the zero-velocity curve. Orbit (b) with the more organized delay plot, ranges more widely, but less randomly, than orbit (a).

5 Thickened Disks

We have so far been investigating force fields which have sharp discontinuities. That is an idealization of a galaxy with a disk-like component, and so one must wonder how critically do the results which we have found depend on the assumption of an abrupt discontinuity. We investigate this issue thickening the disk, borrowing a device introduced by Miyamoto and Nagai [22]. We add a length b, which is zero in the limit of a razor-thin disk, to the definition of the variable ξ on which the potential depends, so that now

$$\Phi = \Phi(\xi), \qquad \xi = \sqrt{R^2 + (a + \sqrt{z^2 + b^2})^2}. \tag{11}$$

This potential is due to the density field

$$\varrho = \frac{1}{4\pi G}\left[\Phi'' + \frac{2\Phi'}{\xi} + \frac{ab^2\Phi'}{\xi(z^2+b^2)^{3/2}} - \frac{b^2}{\xi}\left(\frac{\Phi''}{\xi} - \frac{\Phi'}{\xi^2}\right)\left(1 + \frac{a}{\sqrt{z^2+b^2}}\right)^2\right]. \tag{12}$$

The first three components give the density (3) in the limit $b \to 0$ when $b^2/(z^2 + b^2)^{3/2} \to 2\delta(z)$. The right half of Fig. 2 shows contours of the projected density for the logarithmic potential of (5) when viewed edge-on. Comparison with the unthickened case in the left half shows that there has been a considerable lowering of density contrasts, and that, even though ξ can no longer be interpreted as a specific distance, yet it does tend to a radial distance at large distances where

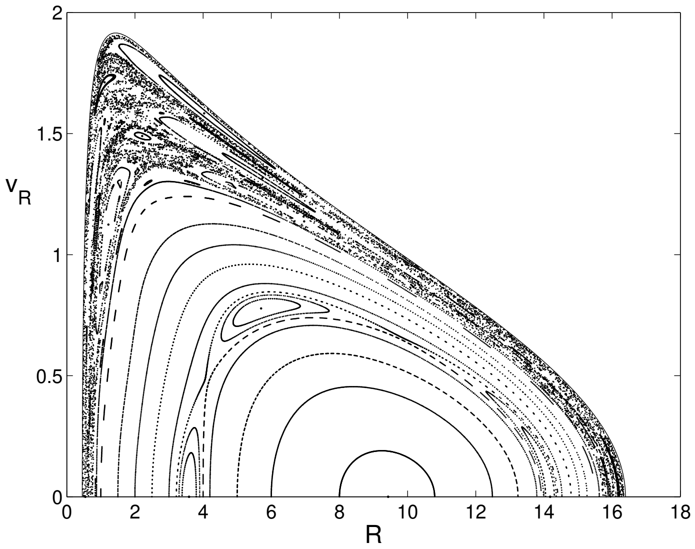

Fig. 14. Surface of section for axisymmetric orbits for $R_c = 10$ and $k = 0.1$, as in Fig. 11 but for a thickened potential with $b = 0.5$

most of the equipotentials become quite spherical. Despite these changes when $b = 0.5$ and so not much smaller than the displacements $a = 1$ of the former centers of force, yet the $R_c = 10$ surface of section, shown in Fig. 14, shows no significant qualitative differences from the $b = 0$ case of Fig. 11. In fact much of the microstructure persists. For example, the small island around $(2.21, 1.49)$ in Fig. 14 and that around $(2.11, 1.46)$ in Fig. 11 are due to similarly shaped $7 : 10$ orbits, and the narrow tadpoles around $(1.11, 1.71)$ in Fig. 14 and $(0.92, 1.62)$ in Fig. 11 are due to similar $5 : 6$ orbits.

6 Discussion and Conclusions

6.1 Related Work

This work adds another example to those already known in which chaos is induced when orbits pass between two or more regions, in each of which the motion is integrable, but in which different integrals apply. One that has attracted considerable attention in recent years is that of a black hole at the center of an otherwise smooth-cored triaxial galaxy. Shortly after de Zeeuw [14] had shown how Stäckel potentials account nicely for the major orbit families which Schwarzschild [23] had found in his numerical integrations of a smooth-cored triaxial galaxy, Gerhard and Binney [24] showed how destructive a central black hole, or cusp, would be for box orbits which came close to it. Motion near the black hole is nearly Keplerian, as has been discussed in detail by Sridhar and Touma [25].

Transitions between regions in which different integrals apply are basic to the mapping constructed by Wisdom [26] to explain the Kirkwood gaps in the asteroid belt. His mapping concentrates high-frequency perturbations by Jupiter into a periodic sequence of impulses which modify the motion periodically. Between impulses, the motion is determined entirely by secular terms which describe an integrable system. Touma and Tremaine [27] have applied a similar mapping in galactic dynamics. They study eccentric orbits in a plane non-axisymmetric potential using a map obtained by concentrating the non-axisymmetry so that it acts impulsively at apocenters of orbits. Between successive apocenters the non-axisymmetry is ignored and the orbital motion is integrable.

From a mathematical perspective, this work adds another instance in which there is evidence that KAM curves occur, even though the conditions for which the KAM theorem has been proved are not satisfied. Moser's [28] proof of that theorem has been refined to the case of continuous derivatives through to third order. Yet Kuzmin-like potentials have discontinuous first derivatives. Like the example of Varvoglis [29], ours comes directly from a significant physical context. Many studies in which KAM curves have been found for Hamiltonians which lack the smoothness required by Moser's proof, such as that of Benettin and Strelcyn [30] have studied variants of the billiard ball problem introduced by Birkhoff [31].

6.2 Conclusions

Our largely numerical study of orbits in Kuzmin-like potentials has shown that Kuzmin's disk is not typical. Its out-of-plane orbits are all integrable, despite the abrupt changes in the angular momentum vector which occur whenever the disk is crossed. Other Kuzmin-like models (other than the simple case in which the potential is harmonic) are not integrable. The presence of the disk causes many more resonances than have been found in similar smooth potentials [32] [17]. Those resonances grow at relatively modest values of energy, overlap, and give rise to many stochastic orbits for which the disk crossings may scatter the angular momentum vector fairly randomly. The extent of the stochasticity grows with increasing energy and decreasing angular momentum. However, there are many orbits which remain regular despite the impulsive changes due to crossing the disk. We have investigated only a very limited class of Kuzmin-like models, and Kuzmin-like models are themselves special because they do not permit the disk density to be adjusted independently of the volume density. Yet it is hard to see why similar mechanisms will not induce stochasticity in disk-crossing orbits in galaxies with disks of substantial size. The similar results from our even more limited tests with thickened Kuzmin-like potentials, for which the disk is not a sharp discontinuity and for which the motion is not integrable outside the disk, is evidence of the likely robustness of our findings. Martinet et al [4]–[7] investigated quite different models. Some of their surfaces of section show large stochastic regions, more extensive than any we display, and even instances in which the central periodic orbit of an axisymmetric case has become unstable.

Because the models are so different, no detailed comparison of our results with theirs is possible.

Although we drew a distinction in Sect. 1 between our interest in orbits and that of Ostriker et al [3] on the internal structure of globular clusters, that distinction may be somewhat fuzzy. The occurrence of chaos is commonly ascribed to sensitivity to initial conditions, when small changes in initial conditions lead to greatly different outcomes [20]. The disruptive effect studied in [3] arises when orbits, which are nearby when viewed on the galactic scale, grow far apart. Our work finds that there are substantial regions of phase space in which orbits remain regular. In them nearby orbits diverge only gradually from each other, whereas in stochastic regions nearby orbits will diverge rapidly from each other. This implies that the vulnerability of a globular cluster to disk shocking is likely to depend considerably on its orbit, as Aguilar, Hut, and Ostriker [33] indeed find.

Acknowledgements

It is a pleasure to thank George Contoupoulos, and Nikos Voglis and his committee, for organizing a stimulating workshop, and for their hospitality. This work has been supported in part by the National Science Foundation through grant DMS-0104751.

References

1. R. Bender, S. Döbereiner, C. Möllenhoff, A&AS, **74**, 385 (1988)
2. C. Scorza, R. Bender, A&A, **293**, 20 (1995)
3. J.P. Ostriker, L. Spitzer, R.A. Chevalier, ApJ, **176**, L51 (1972)
4. L. Martinet, A. Hayli, A&A, **14**, 103 (1971)
5. F. Mayer, L. Martinet, A&A, **27**, 199 (1973)
6. L. Martinet, A&A, **32**, 329 (1974)
7. L. Martinet, F. Mayer, A&A, **44**, 45 (1975)
8. M. Schmidt, Bull. Astron. Inst. Neth., **13**, 15 (1956)
9. M. Schmidt: 'Rotation parameters and distribution of mass in the Galaxy'. In: *Stars and Stellar Systems, Vol. 5* ed. by A. Blaauw, M. Schmidt (University of Chicago Press, Chicago, 1965) pp. 513-530
10. J.E. Tohline, K. Voyages, ApJ, **555**, 524 (2001)
11. G.G. Kuzmin, Astron.Zh., **33**, 27 (1956)
12. J. Binney, S. Tremaine: *Galactic Dynamics* (Princeton University Press, Princeton 1987)
13. H. Goldstein: *Classical Mechanics*, 2nd edn. (Addison-Wesley, Reading MA 1980)
14. P.T. de Zeeuw, MNRAS, **216**, 273 (1985)
15. J. Binney, MNRAS, **201**, 1 (1982)
16. J. Miralda-Escudé, M. Schwarzschild, ApJ, **339**, 752 (1989)
17. C. Hunter, B. Terzić, A.M. Burns, D. Porchia, C. Zink, Ann.N.Y. Acad. Sci., **867**, 61 (1998)
18. O.E. Gerhard, A&A, **151**, 279 (1985)

19. N.H. Packard, J.P. Crutchfield, J.D. Farmer, R.S. Shaw, Phys. Rev. Lett., **45**, 712 (1980)
20. K.T. Alligood, T.D. Sauer, J.A. Yorke: *Chaos: An Introduction to Dynamical Systems* (Springer, New York 1996)
21. M. Schwarzschild, ApJ, **409**, 563 (1993)
22. M. Miyamoto, R. Nagai, PASJ, **27**, 533 (1975)
23. M. Schwarzschild, ApJ, **232**, 236 (1979)
24. O.E. Gerhard, J.J. Binney, MNRAS, **216**, 467 (1985)
25. S. Sridhar, J. Touma, MNRAS, **303**, 483 (1999)
26. J. Wisdom, AJ, **87**, 577 (1982)
27. J. Touma, S. Tremaine, MNRAS, **292**, 905 (1997)
28. J. Moser: *Stable and Random Motions in Dynamical Systems* (Princeton University Press, Princeton 2001)
29. H. Varvoglis, J. Physique, **46**, 495 (1985)
30. G. Benettin, J.-M. Strelcyn, Phys. Rev. A **17**, 773 (1978)
31. G.D. Birkhoff: *Dynamical Systems* (American Mathematical Society, Providence 1927)
32. D.O. Richstone, ApJ, **252**, 496 (1982)
33. L. Aguilar, P. Hut, J.P. Ostriker, ApJ, **335**, 720 (1988)